

EFFICIENT THERMOMECHANICAL SIMULATION FOR METALLIC LATTICE STRUCTURES FABRICATED BY ADDITIVE MANUFACTURING

Natsuki Tsushima^{1,2*}, Masako Kita³, Isamu Matsubara³, Masao Ohishi⁴,

Ryo Higuchi² & Koji Yamamoto³

¹Japan Aerospace Exploration Agency, 6-13-1 Osawa Mitaka Tokyo, 181-0015, Japan
 ²The University of Tokyo, 7-3-1 Hongo, Bunkyo, Tokyo, 113-8656, Japan
 ³Cybernet Systems Co., Ltd., Kanda-neribeicho, Chiyoda, Tokyo, 101-0022, Japan
 ⁴ Ryoyu Systems Co., Ltd., Minato-ku, Nagoya, Aichi, 455-0024, Japan
 ^{*} Corresponding author: +81-70-1170-3148, tsushima.natsuki@jaxa.jp

Abstract

The recent advancement in additive manufacturing (AM) technology has enabled effective realizations of sophisticated structures such as lattice structures. However, if lattice structures are constructed by the AM technique, the geometry of final products slightly differs from its designed geometry although the geometrical precision of the AM technique has greatly improved in recent years. Therefore, it is important to consider the geometrical deviations induced by the AM fabrication. This study aims to investigate the geometrical accuracy and structural characteristics of lattice structures fabricated by AM technique. Thermomechanical simulations are performed to evaluate thermal deformations of lattice structures fabricated by the AM process. Structural characteristics of lattice structures with geometrical predictions of fabricated products are investigated by using a numerical homogenization method. For comparison purposes, tensile lattice specimens were fabricated by using EOS M290 printer. Based on the measurements, distortions in lattice geometries were observed, which would possibly affect the effective stiffnesses of the lattice structures. By considering the influences of the melt pool size and bulge due to the surface tension during the AM process, it was found that those influences on the geometrical deviations in the fabricated lattice structures were significant. In addition, it was confirmed that the estimation for the equivalent material properties of lattice structures could be improved by predicting the actual geometry of lattice unit cells. The present approach would offer effective evaluations of the actual geometry and structural characteristics of a lattice structure. The current approach to predict the actual geometry of lattice structures can also help to optimize process variables to realize the precise geometry of fabricated lattice structures by AM process.

Keywords: Lattice structures, Thermomechanical analysis, Multiscale analysis, Additive manufacturing

1. Introduction

Architected materials have been actively studied as emerging artificial materials for decades. Their distinctive characteristics from other traditional/natural materials can be artificially programmed by the artificial designing of microscopic internal mechanisms [1]. Those materials have shown the potential to improve/extend structural performance and capabilities. Since those artificial materials usually result in complicated geometries, those conceptual designs have faced manufacturing challenges for the realization and production of the materials. However, the recent advancement in additive manufacturing (AM) technology has enabled effective realizations of sophisticated structures that had been conceptual and difficult to fabricate. Mechanical metamaterials can exhibit unique material characteristics and/or behaviors attributed to the micro/mesoscale mechanisms such as truss or porous in addition to constituent material properties constructing the microscopic internal

structures [2-6].

Among a variety of design concepts that have been proposed in the literature [7-9], architected materials based on micro-/meso-scale lattice structures especially provide good compatibility with the AM technique. However, a realization of preferred structural characteristics with structural integrity requires an elaborate design of microscale internal mechanisms in lattice structures. With the complex internal geometry of lattice-based structures, the conventional approach to evaluate the structural characteristics with the finite element method (FEM) by directly modeling designed structures is challenging. Although various topological designs can be precisely evaluated with FEM [10, 11], constructions and simulations of sophisticated models with various geometries result in high costs. In the optimization of internal lattice geometry for a product, finite element models for every possible design are to be constructed even if their microscopic designs are highly complex. Moreover, a simulation of a large-scale structure with lattice-based substructures using a detailed FE model is computationally impractical since such a simulation requires sufficiently small element sizes to obtain accurate FE solutions. In this regard, the multi-scale modeling approach has been developed to evaluate the apparent characteristics of composites by using the computational homogenization method [12-19]. Although the analysis technique originally focused on composite materials, they are reasonably applicable to heterogeneous structures such as architected materials as long as the scale ratio between the microstructure of the materials and the actual structure is sufficiently large. Therefore, the multi-scale modeling approach has been accommodated to evaluate the structural characteristics of lattice-based architected materials by the authors [20].

On the other hand, if lattice structures are constructed by the AM technique, the geometry of final products slightly differs from its designed geometry although the geometrical precision of the AM technique has greatly improved in recent years. The geometrical deviation of additively manufactured structures is mainly caused by thermal deformation during the AM process. To predict the exact geometry of additively manufactured structures, thermomechanical simulations are commonly performed [21, 22]. Geometrical deviations result in different structural characteristics of lattice structures. Therefore, it is important to consider the geometrical deviations induced by the AM fabrication. Since most studies investigating geometrical deviations of additively manufactured structures have focused on simple solid structures, those of lattice structures fabricated by the AM technique have not been fully explored.

This paper studies the geometrical accuracy of lattice structures fabricated by the AM process and its influences on their structural characteristics. We focus on the powder bed fusion (PBF) process, which is one of the popular processes offering compatibility with metal alloys for practical stiffness and strength properties. Thermomechanical simulations are performed to evaluate thermal deformations of lattice structures fabricated by the AM process. Structural characteristics of lattice structures with geometrical predictions of fabricated lattice structures are also investigated by using the numerical homogenization method. For comparison purposes, tensile tests with specimens based on lattice structures are also performed.

2. Numerical Procedure and Theoretical Formulation

In this chapter, a theoretical formulation and numerical procedures for the thermomechanical simulation and the numerical homogenization of lattice structures fabricated by the AM are described briefly. The stiffness and mass properties of a lattice-based structure are effectively evaluated by using the decoupled two-scale numerical procedures.

2.1 Thermomechanical Model

The thermomechanical problems for the AM structures are solved with finite element models by using ANSYS® software based on the element birth and death approach [23]. The transient thermal problem for the AM process is solved based on the conservation of heat equation. The heat equation in the matrix form is given by

$$\overline{C}\dot{T} + \overline{K}T = Q \tag{1}$$

where $\bar{\mathbf{C}}$ is the heat capacity matrix, $\bar{\mathbf{K}}$ is the thermal conductivity matrix, \mathbf{Q} is the heat flow vector, and \mathbf{T} is the temperature vector.

The mechanical problems are solved based on the following governing equation for stress equilibrium

$$\nabla \cdot \mathbf{\sigma} = 0 \tag{2}$$

with the constitutive law as

$$\sigma = C\epsilon_{e} \tag{3}$$

where σ is the stress, C is the elasticity tensor, and ϵ_e is the elastic strain. The total strain ϵ including the thermal strain ϵ_T is given as

$$\epsilon = \epsilon_{e} + \epsilon_{p} + \epsilon_{T} \tag{4}$$

with

$$\boldsymbol{\epsilon}_{\mathsf{T}} = \overline{\boldsymbol{\alpha}} \begin{pmatrix} T - T^{ref} \end{pmatrix} \cdot \begin{bmatrix} 1 & 1 & 1 & 0 & 0 & 0 \end{bmatrix}^{T} \tag{5}$$

where ϵ_p is the plastic strain, $\bar{\alpha}$ is the thermal expansion coefficient, and \mathcal{T}^{ef} is the reference temperature. The thermal histories obtained by each thermal model are used as inputs for Eq.(5).

2.2 Numerical Procedure of Computational Homogenization Method

The stiffness and mass properties of a lattice-based structure are evaluated by using the decoupled two-scale numerical procedures. Figure 1 illustrates the overview of decoupled two-scale modeling of lattice structures. The micro- and macro-scales are introduced for the two-scale analysis. The micro-scale evaluation is performed by modeling components of the lattice with solid elements to take into account the heterogeneous characteristics of the lattice. In macro-scale evaluation, the whole lattice structure is represented as a homogeneous Kirchhoff plate with shell elements. The computational homogenization method for plate [12-19] is incorporated as a scale-up approach to link the two different scales. The homogenization methods provide macroscopic equivalent stiffness of Kirchhoff plate (i.e., the ABD matrix) based on the micro-scale periodic unit cell (PUC) of the lattice structure. Using an effective stiffness, a macroscopic structural simulation can be performed to evaluate the structural performance and integrity of the lattice structures. Note that the deformation of the lattice component is assumed to be small even in the macroscopic large deformation problem. In other words, the geometrical and material nonlinearities are neglected in the micro-scale evaluation.

A lattice-based heterogeneous plate consisting of periodic micro-lattice is considered as shown in Figure 1. Equivalent homogeneous stiffness for Kirchhoff plate of a PUC is obtained based on a three-dimensional solid model of the lattice PUC by using the homogenization method for plates [12-19]. The following micro-scale governing equations are solved in the PUC, as shown in Figure 2.

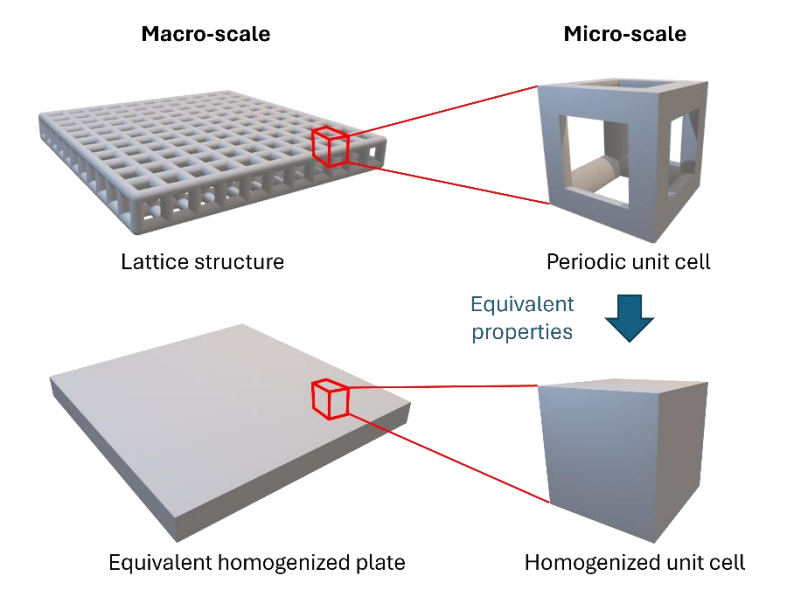


Figure 1 – A concept of computational homogenization for the lattice structure.

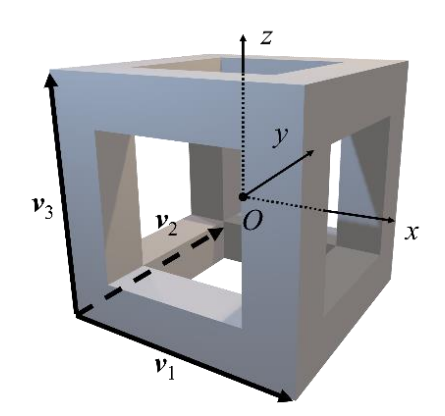


Figure 2 – Illustration of micro-lattice structure in the homogenization method.

$$\frac{\partial \sigma_{ij}}{\partial x_{j}} = 0, \quad \sigma_{ij} = C_{ijkl} \varepsilon_{kl}, \quad \varepsilon_{\alpha\beta} = E_{\alpha\beta}^{0} + x_{3} K_{\alpha\beta}^{0} + \varepsilon_{\alpha\beta}^{(per)}, \quad \varepsilon_{i3} = \varepsilon_{i3}^{(per)}$$

$$\varepsilon_{ij} = \frac{1}{2} \left(\frac{\partial u_{i}}{\partial x_{j}} + \frac{\partial u_{j}}{\partial x_{i}} \right), \quad \varepsilon_{ij}^{(per)} = \frac{1}{2} \left(\frac{\partial u_{i}^{(per)}}{\partial x_{j}} + \frac{\partial u_{j}^{(per)}}{\partial x_{i}} \right) \tag{6}$$

where σ_{ij} , ε_{ij} , and u_i are the microscopic stress, strain, and displacement in the PUC. C_{ijkl} is the stiffness tensor of the material in the lattice component. $E^0_{\alpha\beta}$ and $K^0_{\alpha\beta}$ are the macroscopic in-plane strain and curvature on the reference plane. The microscopic displacement and strain with in-plane periodicity are indicated as $u^{(\text{per})}_i$ and $\varepsilon^{(\text{per})}_{ij}$. Latin indices i, j, k, l range from one to three, while Greek indices α , β , γ , δ take one and two.

Based on the Kirchhoff-Love theory, the macroscopic constitutive relation of the effective anisotropic lattice plate is given as

$$N_{\alpha\beta} = A_{\alpha\beta\gamma\delta} E_{\gamma\delta}^{0} + B_{\alpha\beta\gamma\delta} K_{\gamma\delta}^{0}
M_{\alpha\beta} = B_{\alpha\beta\gamma\delta} E_{\gamma\delta}^{0} + D_{\alpha\beta\gamma\delta} K_{\gamma\delta}^{0}$$
(7)

with

$$N_{\alpha\beta} = \frac{1}{|S|} \int_{V} \sigma_{\alpha\beta} dV, \quad M_{\alpha\beta} = \frac{1}{|S|} \int_{V} \sigma_{\alpha\beta} X_{3} dV$$
 (8)

where $N_{\alpha\beta}$, and $M_{\alpha\beta}$ are the resultant forces and moments. The area of PUC is $|S| = |v_1 \times v_2|$. $A_{\alpha\beta\gamma\delta}$, $D_{\alpha\beta\gamma\delta}$, and $B_{\alpha\beta\gamma\delta}$ are the effective extension, bending, and coupling stiffness tensors. These equivalent stiffnesses are obtained in the following procedure.

- (1) The microscopic stress in the PUC is calculated by assigning the macroscopic unit strain or curvature for the micro-scale problem defined by Eq. (6).
- (2) The components of the effective stiffness tensor are obtained by calculating the macroscopic resultant force and moment with Eq. (8).

The periodic boundary conditions (PBCs) are imposed on the PUC to solve the micro-scale problem given by Eq. (6) [20, 24-26]. In the case of the homogenization for plates, only the x-z and y-z planes of a PUC have periodicity. These procedures are implemented in the pre-and post-processes of the commercial finite element software Abaqus 2019 [27] via the Python script. The numerical homogenization method has been validated by comparing the numerical solutions obtained by the present method and experimental results in the previous works [20, 28].

3. Lattice Structures

In this section, the fabrication of lattice structures by AM is described. The fabricated lattice specimens were then experimentally evaluated in terms of the geometrical accuracy and material properties.

3.1 Fabrication

To investigate the accuracies of thermomechanical simulations, tensile specimens with a PUC of simple cubic lattice were fabricated by using EOS M290 printer, as shown in Figure 3. The specimens were designed as an array of simple cubic (SC) lattice PUCs. The length, width, and thickness of the specimens were 102, 12, and 3 mm, respectively. The dimensions of the PUC were 3 mm x 3 mm x 3 mm. The PUCs consisted of square beams with cross-sections of 0.6 mm x 0.6 mm. Aluminum alloy powder of AlSi10Mg was used. Table 1 lists the printing parameters. The layer thickness, laser power, and laser speed, spot diameter were 30 μ m, 370 W, 1300 mm/s, and 80 μ m, respectively. The specimens were built in the z-direction. Five specimens were fabricated to evaluate the mechanical properties of the specimens with n=5. Young's modulus, Poisson's ratio, and density of structures fabricated with AlSi10Mg power provided by EOS were assumed to be 70 GPa, 0.33, and 2670 kg/m³ based on the material data sheet although they may vary due to the printing parameters.

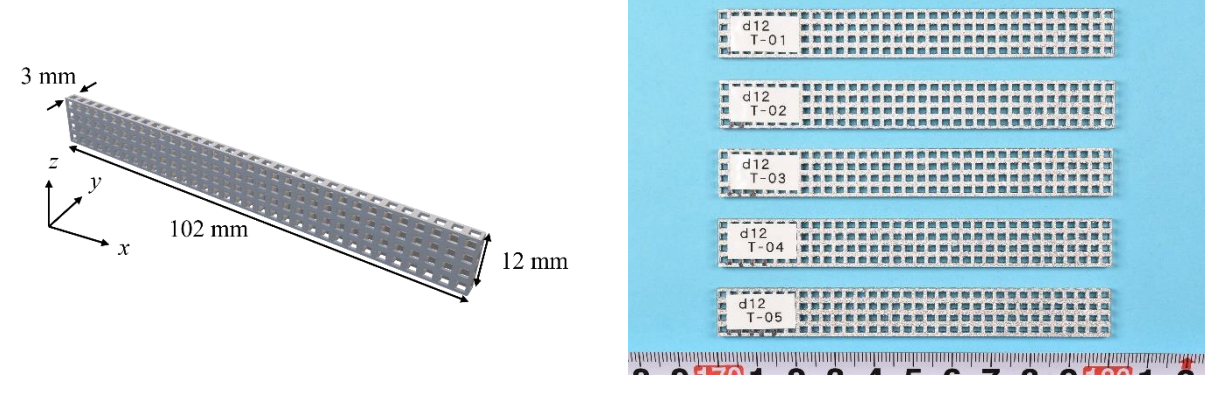


Figure 3 – The geometry of lattice-based specimens (left) and a picture of specimens (right).

Table 1. Printing parameters.

Layer thickness, μm	Laser power, W	Laser speed, mm/s	Spot diameter, μm	
30	370	1300	80	

3.2 Geometrical Accuracy

The geometries of the fabricated specimens were first measured to investigate the geometrical accuracy of lattice structures fabricated by AM. The geometries of a PUC in the specimens were evaluated by assuming the periodicity of the lattice structure although the thermal deformation should have not been exactly periodic over an additively manufactured structure. The geometries of a PUC in the specimens were obtained by using the one-shot 3D measuring microscope (Keyence Corp.). Figure 4 shows the measurement of the first specimen. The cross-sectional geometries of specimens around the middle of the specimens were also obtained by an X-ray computer tomography scanner (TOSCANNER-32300µFPD). As shown in Figure 5, no voids were observed within the specimens. The average length, width, and thickness of the five specimens were 102.2, 12.48, and 2.99 mm, respectively. Table 2 summarizes the averaged geometries of PUC in the specimens. The numbers for the width and thickness of the lattice beams correspond to those in Figure 4. The additively manufactured specimens were precisely fabricated for most of the averaged geometries except there were slight differences in geometries of PUCs. The width of the lattice beams in the layer direction showed the largest discrepancies compared to those in the other directions. Consequently, the shape of the hollow regions in PUCs was distorted. These distortions possibly affect the effective stiffnesses of the lattice structures.

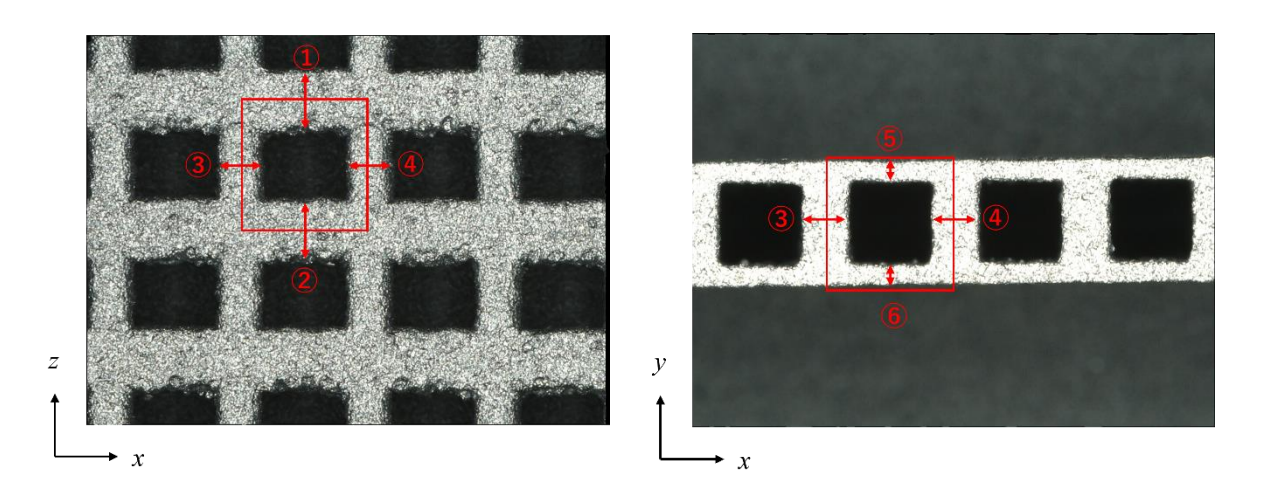


Figure 4 – Geometries of the first specimen on the x-y plane (left) and the x-z plane (right).

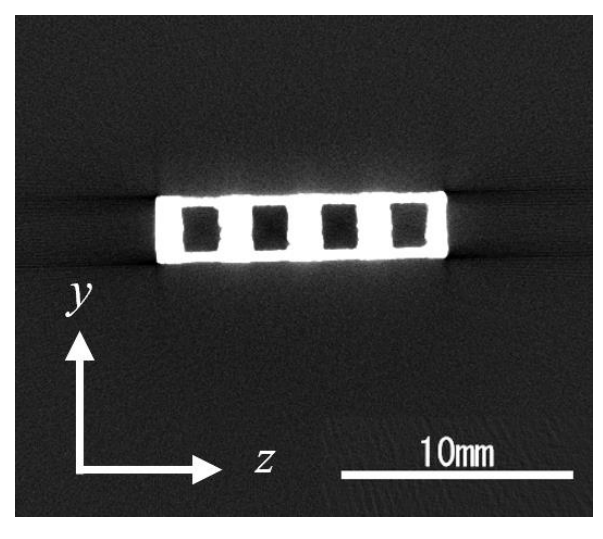


Figure 5 – The cross-section of the first specimen obtained by the CT scan.

Table 2. Averaged geometries of PUC in lattice specimens.

Model	PUC size, mm				Lattice v	width, mm	Lattice thickness, mm		
	Х	У	Z	1	2	3	4	5	6
Original	3.000	3.000	3.000	1.200	1.200	1.200	1.200	0.600	0.600
Actual	3.000	2.871	2.987	1.523	1.519	1.092	1.091	0.508	0.514
Error	0.000	-0.129	-0.013	0.323	0.319	-0.108	-0.109	-0.092	-0.086

3.3 Mechanical Properties

Tensile tests with the lattice specimens were performed to evaluate the mechanical properties of the specimens. The experiments were conducted in accordance with Japanese Industrial Standards (JIS) K7161 for the tensile tests. In the tensile tests, the outer sections from both tip edges to 11 mm were clamped. An extensometer (Instron Corp.) with a 50-mm gauge length was used to measure the strains. Crosshead speeds for the tensile and bending tests were 1.0 mm/min. An extensometer (Instron Corp.) with a 50-mm gauge length was used to measure the strains. Based on the measurements from the tensile tests, the effective stiffnesses of the specimens were calculated. The effective stiffnesses of the specimens were defined by assuming the specimens as equivalent solid structures with the same width and thickness because the lattice-based structures were not simple solid structures. Figure 6 shows the experimental environment for the tensile tests.

Figure 7 shows stress-strain curves of the lattice specimens measured by the tensile experiment. Note that the stress of lattice specimens was calculated as a load divided by an effective cross-sectional area (width x thickness). The results showed consistent linear behaviors in the vicinities of the initial slopes. The variations in plastic and fracture characteristics were owing to differences in the finishing qualities and geometries of the individual specimens. Table 3 summarizes the equivalent tensile properties of the specimens. The values in parentheses indicate the standard deviations. Since the relative density \bar{p} of the current lattice design was 0.352, the equivalent lattice properties could be roughly estimated by the Gibson-Ashby model [29] with $E_{eff} = \bar{p}^g E$. For lattices with ideal bending-dominant behavior, g = 2. Therefore, the Gibson-Ashby model estimated the equivalent tensile modulus of 8.673 GPa, which agreed with the experimental results in some extent. However, it was reported that the model would give deviations in case of a lattice with a low relative density [30]. In addition, the discrepancies in the PUC dimensions must have contributed to the differences in the material properties of the fabricated specimens. Therefore, more detailed evaluations are performed with numerical homogenization.



Figure 6 – Test setup of the tensile and bending experiment.

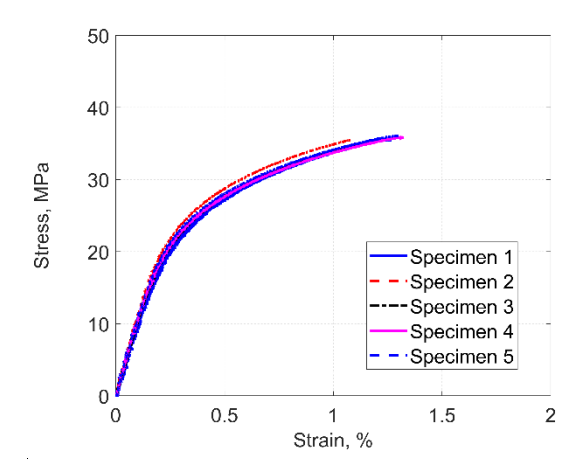


Figure 7 – Stress-strain curves of lattice specimens.

Table 3. Equivalent tensile properties of lattice specimens.

Specimen ID.	Ultimate stress, MPa	Equivalent tensile modulus, GPa
1	35.541	9.782
2	35.471	10.930
3	34.604	8.852
4	35.887	9.420
5	36.121	10.447
Average	35.525 (0.578)	9.886 (0.822)

4. Numerical Studies

In this section, the results of thermomechanical simulations for the lattice structures fabricated by AM are discussed. In addition, the mechanical properties of the fabricated lattice structures were investigated with numerical homogenization by taking the geometrical deviations in the fabricated lattice structures into account.

4.1 Results of Thermomechanical Simulations

Thermomechanical simulations for the lattice specimens were performed with Ansys® MechanicalTM for powder bed fusion (AM LPBF process simulation) [31] to evaluate the thermal deformation of the specimens for the AM process. The results were then compared to the geometries of the fabricated specimens. Figure 8 shows the finite element model of the lattice specimen for the thermomechanical simulations. The hexagonal elements (voxel mesh) with a size of 0.15 mm, which results in 382,976 elements, were used to model the specimen. The model was assumed to be built on the base plate. The heat was applied to super layers, the height of which was 0.15 mm. as the melting temperature of the material. The hatch space, layer thickness, and scan speed were 0.19 mm, 30 μ m, and 1300 mm/s, respectively. The pre-heating and room temperatures were 200 and 22°C. The ambient and powder temperatures were assumed to be the same as the pre-heating temperature. The heat transfer coefficients for the gas and powder were set to 1×10-5 W/(mm·°C). Material properties are varied based on the temperature change by using Ansys's material library.

Figure 9 shows the obtained deformation of the specimen. The numerical results showed that the deformation and warping over the specimen was very small, which agreed with the observation on the fabricated specimens. The deformed shape on a PUC and dimensions of neighboring lattice beams were then evaluated with nodes shown in Figure 10. Table 4 summarizes the averaged displacements due to the thermal deformation and the deformed PUC dimensions. From the result, it could be seen that the deformations of the outer boundary of PUC in the *x* and *z* directions were very small, which also agreed with the measurements in Table 2. However, the amount of the deformation in the *y* direction was three times smaller than those of the fabricated specimens. The thermal deformations of the lattice beams predicted by the thermomechanical simulation were also

much smaller than those of the fabricated specimen.

In the fabricated specimens, the width of the lattice beams in the building direction was larger than those of the designed model. Therefore, there was a possibility that the discrepancy in the PUC dimensions was attributed to the melt pool depth and surface tension. In addition, the relationship between the melt pool dimensions and the beam offset might have impacted the discrepancy in the in-plane dimensions of the fabricated lattice structures. Figure 11 describes images of the contributions for the geometrical difference in the fabricated lattice structures due to the meltpool dimension, surface tension, and beam offset. To further investigate the key contributions of the deformed cell shape on each PUC in the fabricated specimens, the melt pool size based on the printing parameters was evaluated by Ansys® Additve ScienceTM [31]. Table 5 lists the predicted melt pool dimensions in case of the printing on powder and the built plate. The prediction of the melt pool dimensions for the printing configuration on the build plate was used to estimate the melt pool dimensions for the printing on previous layers. The bulge height, as shown in Figure 11, is estimated based on the classical equation of surface tension γ for a sessile drop test [32], which is given by

$$\gamma = f \rho g a^2 b / 6(a - b) \tag{9}$$

where f is a correction factor, ρ and g are the material density and the acceleration of gravity. The variables a and b are the radius of the melt pool and the height of the bulge. We considered that f = 1 in this study. The surface tension of AlSi10Mg in the AM process was assumed to be 0.835 N/m [33]. The density of the melting AlSi10Mg was estimated as 1710 kg/m³ based on the melting temperature at 570°C. Since bulges only occurred on the top layers built on the previous layers, the radius of the melt pool was estimated as 0.133 based on the solution on the build plate (see Table 5). The estimated height of the bulge due to the surface tension was 0.133 mm. Also, the in-plane geometrical deviations on each contour of lattice specimens were estimated as the difference between the radius of the melt pool and the beam offset during the AM process. The same radius of the melt pool (0.133 mm) was used in the estimation as most components of the lattice structure were built on the previous layers. Since the beam offset used to fabricate the lattice specimens was 0.185 mm, the in-plane geometrical deviations were estimated to be 0.0525 mm.

The average geometries of the lattice structures fabricated by the AM process were then calculated as a summation of the simulated thermal deformation, melt pool depth, height of the bulge due to the surface tension, and in-plane geometrical deviations. The predicted geometries were compared with those of the original model and actual specimens in Table 2. Table 7 summarizes the comparison result. Note that the dimensions of the PUC were estimated based on only thermal deformation. The result showed a good agreement between the prediction and the measurement.

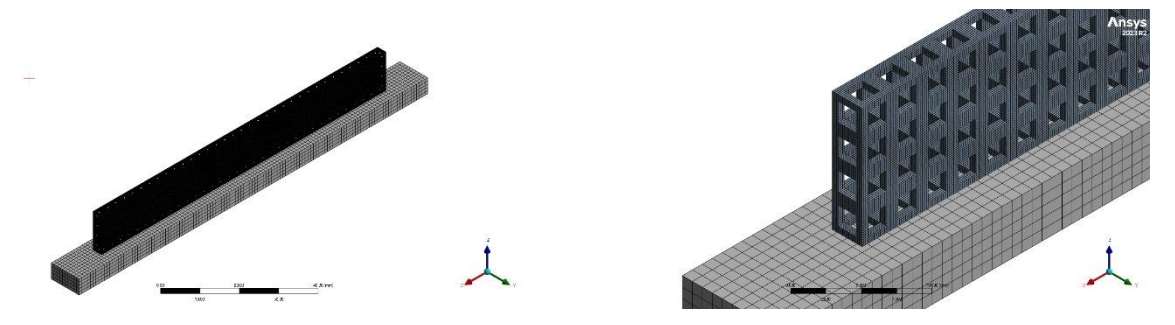


Figure 8 – The finite element models of the lattice specimen for the thermomechanical simulations: the overview (left) and zoomed view (right).

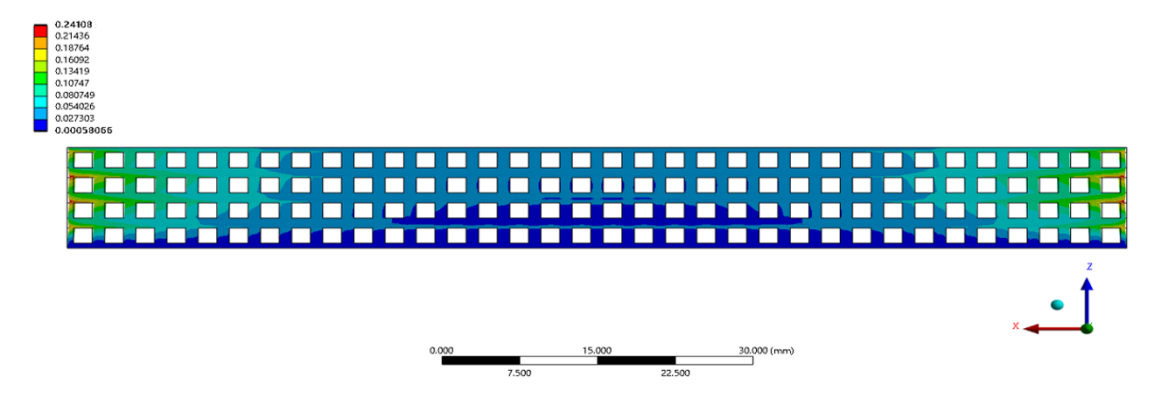


Figure 9 – The deformation of the lattice specimen obtained by the thermomechanical simulation.

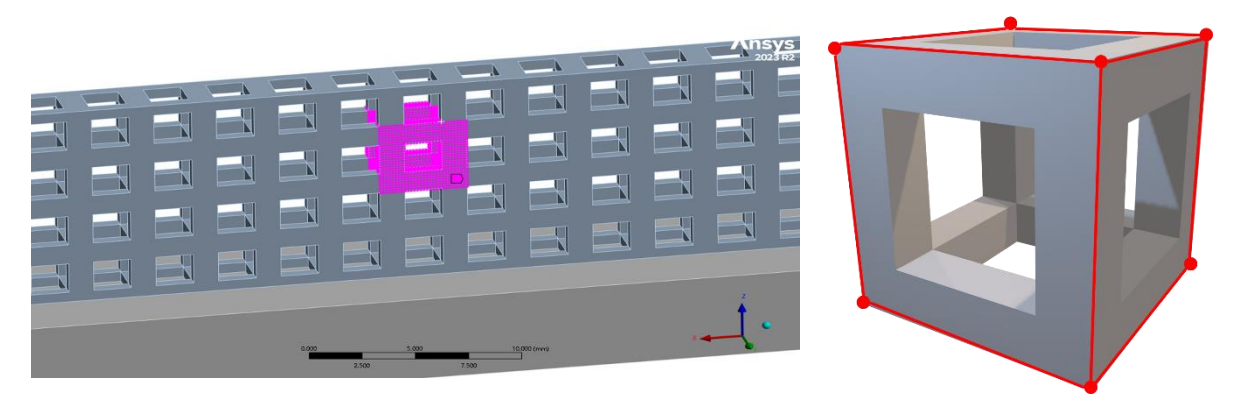
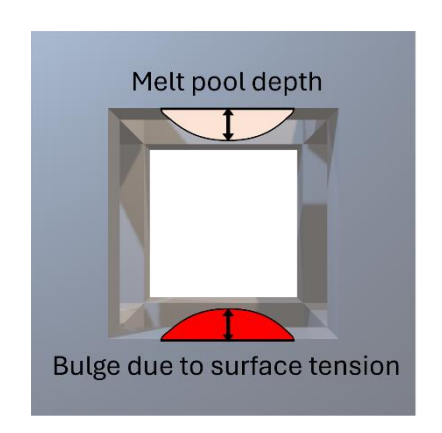


Figure 10 – The measurement locations of deformations on a PUC: nodes on the specimen (left) and the boundary of the PUC (right).

Table 4. Averaged deformed dimensions of the PUC due to the thermal deformation.

Property	PUC size, mm			Lattice width, mm				Lattice thickness, mm	
	Х	у	Z	1	2	3	4	5	6
Deformed shape	2.993	2.962	2.993	1.219	1.218	1.221	1.221	0.615	0.615
Displacement	-0.007	-0.038	-0.007	-0.019	-0.018	-0.021	-0.021	-0.015	-0.015



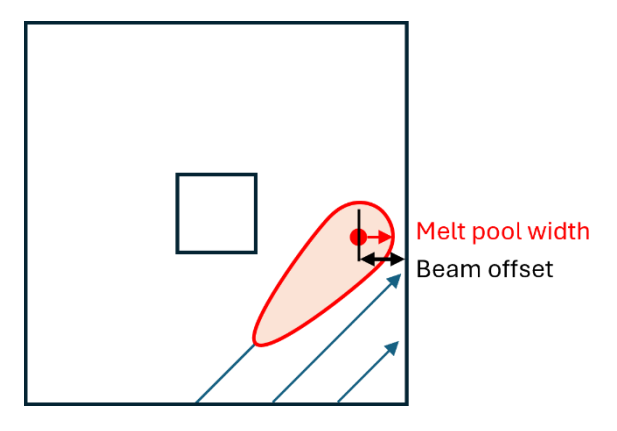


Figure 11 – Images of contributions for the geometrical difference in the fabricated lattice structures due to the meltpool depth/surface tension (left) and the meltpool width and beam offset (right).

Table 5. The dimensions of the melt pool predicted by Ansys® Additive Science™.

Print condition	Depth, mm	Width, mm	Length, mm	
On powder	0.171	0.276	0.504	
On build plate	0.188	0.265	0.486	

Table 6. The height of the bulge due to the surface tension and its related parameters for AlSi10Mg.

Property	Value
Correction factor f	1.0
Density at melting temperature, kg/m ³	1710
Radius of melt pool a, mm	0.133
Surface tension of melting AlSi10Mg, N/m	0.835
Bulge height, mm	0.133

Table 7. Comparison of averaged geometries of PUC in lattice specimens.

Model	PUC size, mm			Lattice width, mm				Lattice thickness, mm	
	Х	у	Z	1	2	3	4	5	6
Original	3.000	3.000	3.000	1.200	1.200	1.200	1.200	0.600	0.600
Actual	3.000	2.871	2.987	1.523	1.519	1.092	1.091	0.508	0.514
Predicted	2.993	2.962	2.993	1.522	1.522	1.116	1.116	0.510	0.510

4.2 Results of Numerical Homogenization

The equivalent stiffnesses of the lattice specimens with the original and predicted geometries were evaluated by numerical homogenization. The solutions were compared with the results obtained by the tensile tests. Figure 12 shows the finite element models for each case. The models were constructed with solid hexagonal elements. The element size of 0.05 mm was used due to computational limitations. Figure 13 shows the comparison result. The error bars for the solutions depict the equivalent Young's moduli with different Young's moduli of AlSi10Mg power. In the current simulation, Young's modulus and Poisson's ratio of lattice structures fabricated with AlSi10Mg power provided by EOS were mainly assumed to be 70 GPa based on the material data sheet. However, it is specified that the properties may vary ±10 GPa from the value. Therefore, the minimum values of the error bars were calculated with the Young's modulus of 60 GPa. The error bar of the experimental results denotes the minimum and maximum values obtained by the tensile experiment. Note that the development of local microstructures in lattice structures may vary from those of the bulk solid structures in the AM process due to different thermal histories, which results in deviations in local material properties. Those influences were not considered in the current study. According to the comparison result, the equivalent Young's modulus based on the Young's modulus of 60 GPa with the actual geometry of the fabricated lattice structure was in the range of the error bar for the experimental results. The differences of the equivalent Young's moduli obtained by the homogenization with the original and predicted geometries of the fabricated lattice specimens to the equivalent Young's modulus with the actual geometry were 0.004% and 2.2% respectively. Therefore, the estimation for the equivalent material properties of lattice structures could be improved by predicting the actual geometry of lattice PUCs with the current approach. If accurate material properties could be obtained, the estimation can be further improved. Such investigations will be performed in future works. The current approach to predict the actual geometry of lattice structures could also help to optimize process variables to realize precise geometry of fabricated lattice structures by AM process.

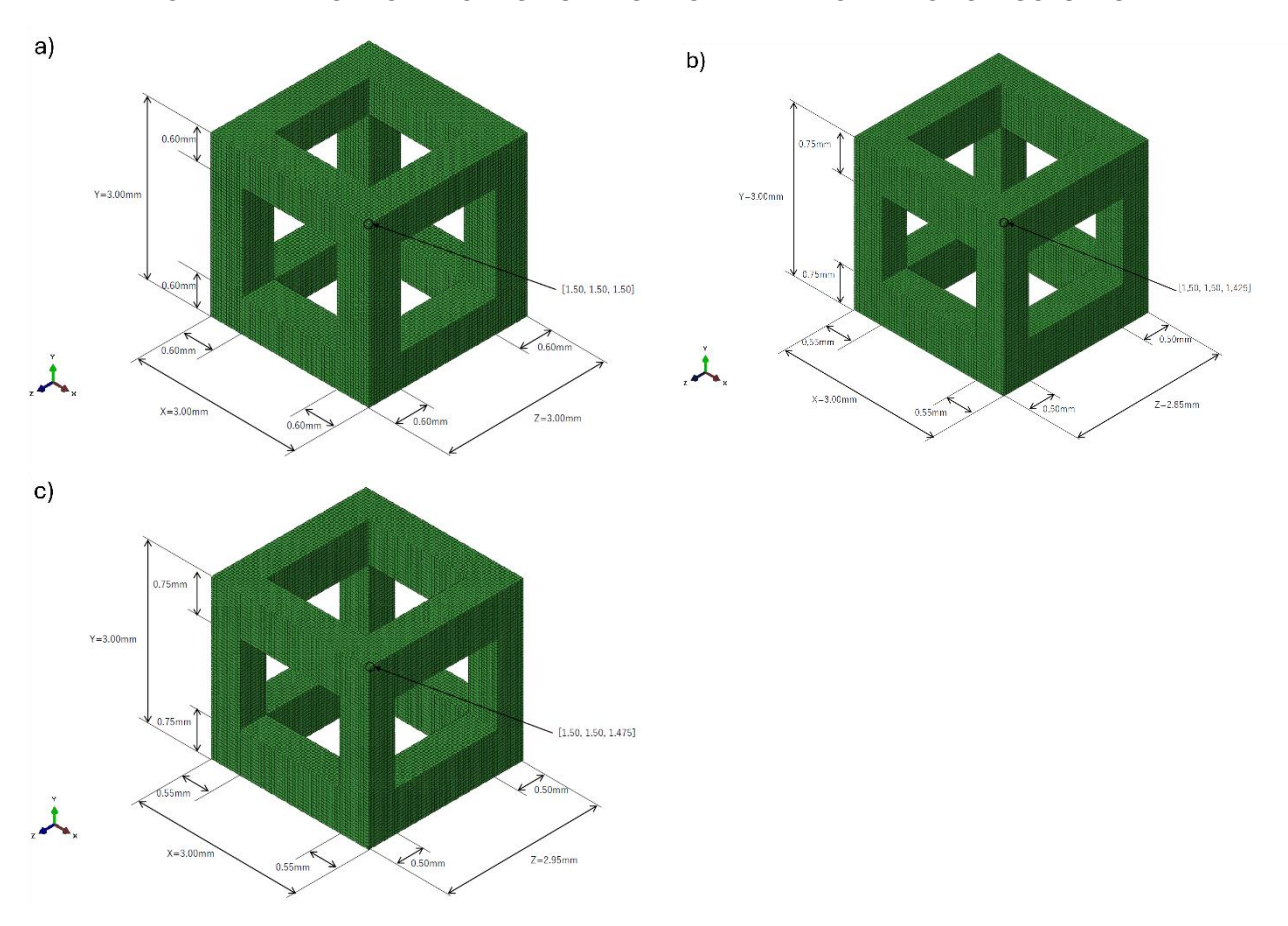


Figure 12 – Finite element models of the lattice specimens: with a) the original, b) actual, c) and predicted geometries.

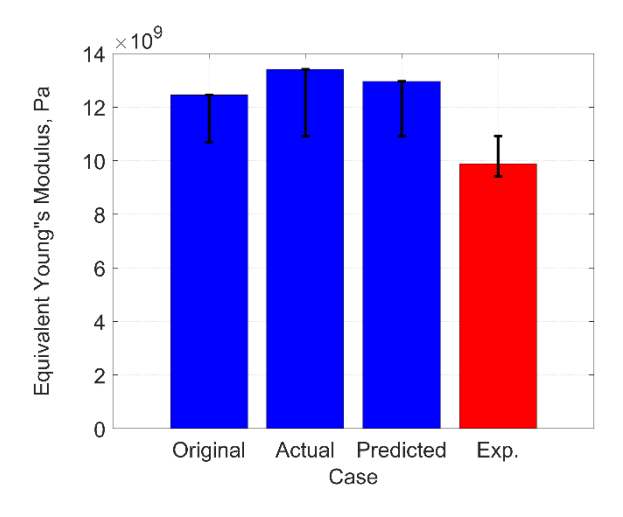


Figure 13 – Comparison of equivalent Young's moduli.

5. Conclusion

This study aimed to investigate the geometrical accuracy and structural characteristics of lattice structures fabricated by the AM process. We focused on the PBF process, which is one of the popular processes offering compatibility with metal alloys for practical stiffness and strength properties. Thermomechanical simulations were performed to evaluate thermal deformations of lattice structures fabricated by the AM process. Structural characteristics of lattice structures with geometrical predictions of fabricated lattice structures were also investigated by using the numerical homogenization method. For comparison purposes, tensile test specimens with PUCs of the SC lattice were fabricated by using EOS M290 printer. The experimental results were then compared with the numerical solutions.

Based on the measurements, it was observed that the additively manufactured specimens were precisely fabricated for most of the averaged geometries except there were slight differences in the geometries of PUCs. The width of the lattice beams in the layer direction showed the largest discrepancies compared to those in the other directions. Consequently, the shape of the hollow regions in PUCs was distorted. These distortions would possibly affect the effective stiffnesses of the lattice structures.

According to the thermomechanical solution for the lattice specimens obtained by Ansys® MechanicalTM for powder bed fusion (AM LPBF process simulation), the thermal deformations of the lattice beams predicted only by the thermomechanical simulation were much smaller than those of the fabricated specimen. Based on further investigation by considering the influences of the melt pool size and bulge due to the surface tension during the AM process, it was found that those influences on the geometrical deviations in the fabricated lattice structures were significant. In addition, it was confirmed that the estimation for the equivalent material properties of lattice structures could be improved by predicting the exact geometry of lattice PUCs.

The present approach would offer effective evaluations of the actual geometry and structural characteristics of a lattice structure. If accurate material properties could be obtained, the estimation can be further improved. Such investigations will be performed in future works. The current approach to predict the actual geometry of lattice structures can also help to optimize process variables to realize the precise geometry of fabricated lattice structures by AM process. In the current study, the bulge size was simply estimated by the classical formulation. However, a more detailed evaluation based on computational fluid dynamics will also be performed in future works.

6. Contact Author Email Address

Corresponding author: Natsuki Tsushima, tsushima.natsuki@jaxa.jp

7. Copyright Statement

The authors confirm that they, and/or their company or organization, hold copyright on all of the original material included in this paper. The authors also confirm that they have obtained permission, from the copyright holder of any third party material included in this paper, to publish it as part of their paper. The authors confirm that they give permission, or have obtained permission from the copyright holder of this paper, for the publication and distribution of this paper as part of the ICAS proceedings or as individual off-prints from the proceedings.

References

- [1] Berger JB, Wadley HNG, and McMeeking RM, Mechanical Metamaterials at the Theoretical Limit of Isotropic Elastic Stiffness. *Nature*, Vol. 543, pp. 533–537, 2017.
- [2] Wu W, Hu W, Qian G, Liao H, Xu X, and Berto F, Mechanical Design and Multifunctional Applications of Chiral Mechanical Metamaterials: A Review. *Materials & Design*, Vol. 180, p. 107950, 2019.
- [3] Qureshi A, Li B, and Tan KT, Numerical Investigation of Band Gaps in 3d Printed Cantilever-in-Mass Metamaterials. *Scientific Reports*, Vol. 6, No. 1, p. 28314, 2016.
- [4] Tan KT, Huang HH, and Sun CT, Blast-Wave Impact Mitigation Using Negative Effective Mass Density Concept of Elastic Metamaterials. *International Journal of Impact Engineering*, Vol. 64, pp. 20-29, 2014.
- [5] Wang H, Zhang Y, Lin W, and Qin QH, A Novel Two-Dimensional Mechanical Metamaterial with Negative Poisson's Ratio. *Computational Materials Science*, Vol. 171, p. 109232, 2020.
- [6] Ye M, Gao L, and Li H, A Design Framework for Gradually Stiffer Mechanical Metamaterial Induced by Negative Poisson's Ratio Property. *Materials & Design*, Vol. 192, p. 108751, 2020.
- [7] Bauer J, Meza LR, Schaedler TA, Schwaiger R, Zheng X, and Valdevit L, Nanolattices: An Emerging Class of Mechanical Metamaterials. *Advanced Materials*, Vol. 29, No. 40, pp. 1701850 (1-26), 2017.
- [8] Yuan S, Shen F, Bai J, Chua CK, Wei J, and Zhou K, 3d Soft Auxetic Lattice Structures Fabricated by Selective Laser Sintering: Tpu Powder Evaluation and Process Optimization. *Materials & Design*, Vol. 120, pp. 317-327, 2017.
- [9] Maconachie T, Leary M, Lozanovski B, Zhang X, Qian M, Faruque O, and Brandt M, Slm Lattice Structures: Properties, Performance, Applications and Challenges. *Materials & Design*, Vol. 183, p.

- [10]Xiao Z, Yang Y, Xiao R, Bai Y, Song C, and Wang D, Evaluation of Topology-Optimized Lattice Structures Manufactured Via Selective Laser Melting. *Materials & Design*, Vol. 143, pp. 27-37, 2018.
- [11]Mizzi L, Attard D, Gatt R, Farrugia PS, and Grima JN, An Analytical and Finite Element Study on the Mechanical Properties of Irregular Hexachiral Honeycombs. *Smart Materials and Structures*, Vol. 27, No. 10, p. 105016, 2018.
- [12]Caillerie D, and Nedelec JC, Thin Elastic and Periodic Plates. *Mathematical Methods in the Applied Sciences*, Vol. 6, No. 1, pp. 159-191, 1984.
- [13]Kohn RV, and Vogelius M, A New Model for Thin Plates with Rapidly Varying Thickness. *International Journal of Solids and Structures*, Vol. 20, No. 4, pp. 333-350, 1984.
- [14]Kohn RV, and Vogelius M, A New Model for Thin Plates with Rapidly Varying Thickness. II: A Convergence Proof. *Quarterly of Applied Mathematics*, Vol. 43, No. 1, pp. 1-22, 1985.
- [15]Kohn RV, and Vogelius M, A New Model for Thin Plates with Rapidly Varying Thickness. III: Comparison of Different Scalings. *Quarterly of Applied Mathematics*, Vol. 44, No. 1, pp. 35-48, 1986.
- [16]Lewinski T, and Telega JJ, *Plates, Laminates, and Shells: Asymptotic Analysis and Homogenization*, World Scientific, Singapore, 2000.
- [17]Schmitz A, and Horst P, A Finite Element Unit-Cell Method for Homogenised Mechanical Properties of Heterogeneous Plates. *Composites Part A: Applied Science and Manufacturing*, Vol. 61, pp. 23-32, 2014
- [18] Terada K, Hirayama N, Yamamoto K, Muramatsu M, Matsubara S, and Nishi S, Numerical Plate Testing for Linear Two-Scale Analyses of Composite Plates with in-Plane Periodicity. *International Journal for Numerical Methods in Engineering*, Vol. 105, No. 2, pp. 111-137, 2016.
- [19]Yoshida K, and Nakagami M, Numerical Analysis of Bending and Transverse Shear Properties of Plain-Weave Fabric Composite Laminates Considering Intralaminar Inhomogeneity. *Advanced Composite Materials*, Vol. 26, No. 2, pp. 135-156, 2017.
- [20]Tsushima N, and Higuchi R, Stiffness and Strength Evaluation of Lattice-Based Mechanical Metamaterials by Decoupled Two-Scale Analysis. *Materials Today Communications*, Vol. 31, p. 103598, 2022.
- [21]Burkhardt C, Steinmann P, and Mergheim J, Thermo-Mechanical Simulations of Powder Bed Fusion Processes: Accuracy and Efficiency. *Advanced Modeling and Simulation in Engineering Sciences*, Vol. 9, No. 1, p. 18, 2022.
- [22] Denlinger ER, Irwin J, and Michaleris P, Thermomechanical Modeling of Additive Manufacturing Large Parts. *Journal of Manufacturing Science and Engineering*, Vol. 136, No. 6, 2014.
- [23] ANSYS I, Ansys Mechanical Apdl Theory Reference, Release 2024 R1, Canonsburg, PA, 2024.
- [24]Terada K, Kato J, Hirayama N, Inugai T, and Yamamoto K, A Method of Two-Scale Analysis with Micro-Macro Decoupling Scheme: Application to Hyperelastic Composite Materials. *Computational Mechanics*, Vol. 52, No. 5, pp. 1199–1219, 2013.
- [25] Higuchi R, Yokozeki T, Nagashima T, and Aoki T, Evaluation of Mechanical Properties of Noncircular Carbon Fiber Reinforced Plastics by Using Xfem-Based Computational Micromechanics. *Composites Part A: Applied Science and Manufacturing*, Vol. 126, p. 105556, 2019.
- [26] Higuchi R, Aoki R, Yokozeki T, and Okabe T, Evaluation of the in-Situ Damage and Strength Properties of Thin-Ply Cfrp Laminates by Micro-Scale Finite Element Analysis. *Advanced Composite Materials*, Vol. 29, No. 5, pp. 475-493, 2020.
- [27] Dassault Systems, Abaqus 2019 Documentation, Providence, RI, 2019.
- [28] Tsushima N, Higuchi R, and Yamamoto K, Correlation Studies of Different Decoupled Two-Scale Simulations for Lattice Structures. *Aerospace*, Vol. 10, No. 8, p. 723, 2023.
- [29] Gibson LJ, Cellular Solids. MRS Bulletin, Vol. 28, No. 4, pp. 270-274, 2003.
- [30]Zhong H, Song T, Li C, Das R, Gu J, and Qian M, The Gibson-Ashby Model for Additively Manufactured Metal Lattice Materials: Its Theoretical Basis, Limitations and New Insights from Remedies. *Current Opinion in Solid State and Materials Science*, Vol. 27, No. 3, p. 101081, 2023.
- [31]ANSYS, Ansys, Additive Print and Science User's Guide, Release 2024 R1, Canonsburg, PA, 2024.
- [32]Monma K, and Suto H, Experimental Studies on the Surface Tension of Molten Metals and Alloys. *Transactions of the Japan Institute of Metals*, Vol. 1, No. 2, pp. 69-76, 1960.
- [33]Biffi CA, Bassani P, Fiocchi J, Giuranno D, Novakovic R, Tuissi A, and Ricci E, Investigation of High Temperature Behavior of Alsi10mg Produced by Selective Laser Melting. *Materials Chemistry and Physics*, Vol. 259, p. 123975, 2021.